Revision 1, Word Count 5545

Thermal conductivity of aluminous garnets in Earth's deep interior

Yu-Ping Grace Hung[1, 2†], Yi-Chi Tsao[1], Chun-Hung Lin[1], and Wen-Pin Hsieh[1, 2*]

[1]*Institute of Earth Sciences, Academia Sinica, Taipei 11529, Taiwan*

[2]*Department of Geosciences, National Taiwan University, Taipei 10617, Taiwan*

Abstract

Aluminous garnets [$(Mg,Fe,Ca)_3Al_2(SiO_4)_3$] are a key mineral group in Earth's interior. Their thermal conductivity under relevant chemical compositions and high pressure-temperature (*P-T*) conditions plays a crucial role in affecting the thermal states of pyrolitic mantle and subducted basaltic crust over the depth range they are present. Using ultrafast optical pump-probe spectroscopy combined with an externally-heated diamond anvil cell, we have precisely determined the high *P-T* thermal conductivity of aluminous garnets, including pyrope, grossular, and pyrope-almandine solid solution. We find that the variable chemical composition has minor effects on the thermal conductivity of these garnets over the *P-T* range we studied. Combined with previous results, we provide new depth-dependent thermal conductivity profiles for a pyrolitic mantle and a subducted basaltic crust. These important results significantly benefit geodynamics simulations and advance our understanding of the thermal structure and evolution dynamics in Earth's upper mantle and transition zone. In addition, as garnets are also a key, useful material family for modern technology, our results on the thermal property of natural garnets also shed lights on the novel design of optical and electronic devices based on a variety of synthetic nonsilicate garnets.

Key words: high pressure, thermal conductivity, garnet, geodynamics

†deceased

*Correspondence: wphsieh@earth.sinica.edu.tw

Introduction

Physical and chemical properties (including transport properties) of Earth materials critically determine the seismic profile, thermochemical structure, and evolution dynamics of our planet. Among the constituting minerals in Earth's upper mantle, garnet with a typical chemical formula $(Mg, Fe, Ca, Mn)_3(Al, Fe, Cr)_2(SiO_4)_3$ and space group *Ia3̄d* is of particular importance. Over the depth range where the garnet is present in the upper mantle and subducting slabs, it is expected to form ~15–40 vol% of the pyrolitic mantle (Ringwood 1991) and ~25–90 vol% of the basaltic crust of a subducting slab (Ono et al. 2001). Furthermore, under the peridotitic model, the garnet aggregate is majorly composed of $Mg_3Al_2(SiO_4)_3$ pyrope (~75 vol%) along with $Fe_3Al_2(SiO_4)_3$ almandine (~15 vol%) and $Ca_3Al_2(SiO_4)_3$ grossular (~10 vol%) (Wood et al. 2013). Physicochemical properties of these end-member aluminous garnets (hereafter referred to as Al-garnets) thus play an important role in representing properties of the garnet solid solutions with variable chemical composition in Earth's deep interior.

To understand how the Al-garnets influence the chemical composition, density, seismic structure, and dynamics of the mantle as well as the fate of subducting slabs, in the past decades a number of physical properties of Al-garnets under relevant pressure-temperature (*P*-*T*) conditions have been extensively investigated, including phase stability (Haselton and Newton 1980; Gréaux

et al. 2011b; Kawai and Tsuchiya 2012, 2015), equation of state (Gréaux et al. 2011a; Kawai and Tsuchiya 2012, 2015; Fan et al. 2017), elastic constant and sound velocity (Babuška et al. 1978; Conrad et al. 1999; Jiang et al. 2004; Kono et al. 2010; Kawai and Tsuchiya 2012, 2015; Erba et al. 2014; Arimoto et al. 2015; Hu et al. 2016; Duan et al. 2019), electrical conductivity (Dai and Karato 2009), vibrational spectrum (Hofmeister and Chopelas 1991; Gillet et al. 1992; Kolesov and Geiger 1998), and thermodynamic properties (Hofmeister and Chopelas 1991; Giesting et al. 2004; Galkin and Gartvich 2015; Baima et al. 2016; Hu et al. 2016; Duan et al. 2019), etc. Interestingly, it was found that the end-member composition has little effects on many of the aforementioned properties, such as the density, sound velocity, elastic moduli, and heat capacity, see, e.g., (Haselton and Newton 1980; Hofmeister and Chopelas 1991; Duan et al. 2019). Such results would imply that these properties of the end-member Al-garnets could be used to describe or model those of the complex solid solutions.

Thermal conductivity, the ability to conduct heat, of minerals under relevant high *P-T* conditions is a key transport property to control the thermal evolution and geodynamics in Earth's interior (Xu et al. 2004; Ohta et al. 2012, 2017; Hofmeister and Branlund 2015; Hsieh et al. 2017, 2018, 2022a; Y. Zhang et al. 2019; Guo et al. 2022; Zhang et al. 2022). Such crucial property of garnets, however, had only been studied at relatively low pressure and a wide range of temperature conditions, see, e.g., (Horai 1971; Slack and Oliver 1971; Osako et al. 2004; Hofmeister 2006; Marquardt et al. 2009; Hofmeister and Branlund 2015). As a result, previous numerical modellings on the dynamics of the mantle and slab subduction have often assumed that the thermal conductivity of garnets along relevant high *P-T* conditions is either a constant (Davies 1988; Eberle et al. 2002) or that of olivine (Hsieh et al. 2022a, 2022b), which may lead to incomplete understanding of the thermochemical state and evolution in Earth's interior. A

systematic study on the thermal conductivity of Al-garnets with representative chemical compositions under *P-T* conditions relevant to the pyrolitic mantle and subducting slabs is therefore critically needed. In addition, prior studies have shown that the presence of water in nominally anhydrous mantle minerals, such as olivine (Chang et al. 2017; B. Zhang et al. 2019) and ringwoodite (Marzotto et al. 2020), could reduce their thermal conductivity, which in turn influences the temperature profile and stability zone of minerals in the region. Given the potential water storage capacity of Al-garnets (e.g., ~few hundred wt. ppm in pyrope and ~1 wt. % in grossular) (Jacobsen 2006), characterizing the effects of hydration on the thermal conductivity of representative Al-garnets at extreme conditions is of great importance, while it remains largely unknown.

In this work, we report the lattice thermal conductivity of $Mg_3Al_2(SiO_4)_3$ pyrope, $(Ca_{0.986}Fe_{0.014})_3Al_2(SiO_4)_3$ grossular, and $(Mg_{0.44}Fe_{0.45}Ca_{0.1}Mn_{0.01})_3Al_2(SiO_4)_3$ pyrope-almandine solid solution at high *P-T* conditions relevant to the Earth's upper mantle and subducting oceanic crust. We find that the thermal conductivity of these garnet phases is insensitive to its complex end-member chemical substitutions; furthermore, it is smaller than the thermal conductivity of dry olivine (Chang et al. 2017) and ringwoodite (Marzotto et al. 2020), at odds with conventional assumptions. More importantly, our findings combined with literature results enable more comprehensive data modeling on the thermal conductivity evolution of the pyrolitic mantle and subducting slab, significantly advancing numerical simulations on the dynamics and thermochemical evolution in Earth's deep interior where the garnets are present.

Experimental Methods

Sample preparation

93 The hydrous pyrope sample was synthesized by a large volume press in National Cheng Kung
94 University, Taiwan. The starting materials of $Mg(OH)_2$, Al_2O_3, and SiO_2 were well-mixed,
95 compressed to 4 GPa, and heated to 1200 C for 10 hours, followed by a ~30-minute quench to
96 room temperature. Natural samples of grossular and pyrope-almandine solid solution originated
97 from Mexico and Sri Lanka, respectively, were commercially purchased from a local mineral
98 company in Taiwan. Using the electron probe microanalyzer in Academia Sinica, the chemical
99 composition for each garnet was determined to be $Mg_3Al_2(SiO_4)_3$ for pyrope,
100 $(Ca_{0.986}Fe_{0.014})_3Al_2(SiO_4)_3$ for grossular, and $(Mg_{0.44}Fe_{0.45}Ca_{0.1}Mn_{0.01})_3Al_2(SiO_4)_3$ for pyrope-
101 almandine solid solution. The water content in each sample was characterized by Fourier
102 Transform Infrared (FTIR) spectroscopy, see (Chang et al. 2017) for the details of our FTIR
103 measurements and analysis for the absorbance. For each sample, we performed FTIR
104 measurements on multiple locations over the sample, which showed reasonably consistent
105 absorption spectra, indicating the water distribution among the sample is fairly homogeneous. Our
106 data suggested that the pyrope and grossular contain ~700 and ~5500 wt. ppm water, respectively,
107 while the pyrope-almandine sample is essentially dry.
108 To prepare the samples for thermal conductivity measurements at high pressure and room
109 temperature, each garnet sample was first manually polished to a thickness of ~20 μm, and then
110 thermally evaporated with an Al thin film (~90 nm-thick), serving as the thermal transducer. The
111 garnet sample and several ruby spheres were loaded into a symmetric DAC (500 μm culet) with a
112 Re gasket, and compressed by loading silicone oil (CAS No. 63148-62-9 from ACROS
113 ORGANICS) as the pressure medium. The pressure within the DAC was characterized by the
114 pressure-induced fluorescence shift of ruby balls (Dewaele et al. 2004) with a typical uncertainty
115 of <5% over the pressure range we studied.

We used an externally heated DAC (EHDAC) (Hsieh 2021) to generate simultaneous high *P-T* conditions. Here the garnet sample was compressed by high-pressure gas loading of Ar (purity of 99.9999%) as the pressure medium. Note that our EHDAC was equipped with a gas membrane which enabled *in situ* control on the experimental pressure within the EHDAC and thus a precise probe of the temperature dependence of thermal conductivity of garnets at a fixed pressure. Detailed experimental setup, sample geometry, and the EHDAC assemblage and temperature measurement had been shown elsewhere, see, e.g., (Hsieh et al. 2009; Hsieh 2021).

Thermal conductivity measurements and data analysis

Thermal conductivity of garnets at high pressure and a wide range of high temperature conditions were measured by time-domain thermoreflectance (TDTR). TDTR is an ultrafast optical pump-probe technique that enables high-precision thermal conductivity measurements on a variety of materials under different length scale and pressure-temperature conditions (Cahill et al. 2014; Hsieh et al. 2018, 2020; Hsieh 2021). It utilizes an optical pump pulse to induce a heat wave propagating through the material of interest, and a probe pulse to monitor the heat diffusion dynamics that is partially controlled by the thermal conductivity of the material. The detailed operation principle and experimental setup can be found in literatures, e.g., (Cahill 2004; Kang et al. 2008; Hsieh et al. 2009; Hsieh 2021).

To determine the thermal conductivity of garnets, the TDTR data were fitted by a bi-directional thermal model that simulated heat diffusion from the heated Al transducer to the garnet sample and pressure medium. Details of the thermal model and its parameters under relevant high *P-T* conditions were described in (Schmidt et al. 2008; Hsieh et al. 2009; Chen et al. 2011; Hsieh 2021). A representative TDTR spectrum for pyrope-almandine solid solution at 23.1 GPa and

This is the peer-reviewed, final accepted version for American Mineralogist, published by the Mineralogical Society of America.
The published version is subject to change. Cite as Authors (Year) Title. American Mineralogist, in press.
DOI: https://doi.org/10.2138/am-2023-8953. http://www.minsocam.org/

room temperature fitted by the thermal model is shown in Supplementary Information Fig. S1. In the thermal model fitting, the volumetric heat capacity, C, of the garnet sample is an important parameter. For pyrope and grossular, assuming the relatively small water content has minor effects on the heat capacity, at ambient conditions, C_{pyrope}=2.38 J cm^{-3} K^{-1} from (Hu et al. 2016) and $C_{grossular}$=2.67 J cm^{-3} K^{-1} from (Duan et al. 2019); their changes at high P-T conditions were also taken from (Hu et al. 2016) and (Duan et al. 2019), respectively. By an interpolation between the pure pyrope (2.38 J cm^{-3} K^{-1}) (Hu et al. 2016) and pure almandine (2.96 J cm^{-3} K^{-1}) (Galkin and Gartvich 2015), we estimated the heat capacity of $(Mg_{0.44}Fe_{0.45}Ca_{0.1}Mn_{0.01})_3Al_2(SiO_4)_3$ pyrope-almandine solid solution $C_{pyrope\text{-}almandine}$=2.67 J cm^{-3} K^{-1} at ambient conditions; the $C_{pyrope\text{-}almandine}$ at high P-T conditions was estimated following methods developed in (Hsieh et al. 2009). The thermal conductivity and heat capacity of Ar (used as the pressure medium) in high P-T measurements were taken from (Hsieh et al. 2009, 2022c) . We emphasize that the uncertainty in the thermal conductivity data is majorly from the data analysis, not from the measurements. For instance, the uncertainties in all the parameters involved in our thermal model were estimated to translate an error of ~8% before 10 GPa and ~15% at 10–25 GPa in the garnets' thermal conductivity. More details of the data analysis and uncertainty evaluations are shown in Supplementary Information Fig. S1, Fig. S2, Table S1, and related literatures (Hsieh et al. 2009; Hsieh 2021).

Results and discussions

Figure 1(a) shows the pressure dependence of thermal conductivity Λ of Al-garnets with three chemical compositions at room temperature. Though the chemical composition of our Al-garnets are not the same as those reported previously, their ambient thermal conductivity values

are overall in good agreement with literature results (Horai 1971; Slack and Oliver 1971; Osako et al. 2004; Hofmeister 2006; Marquardt et al. 2009). The dry (black circles) and ~700 wt. ppm water-bearing (red circles) single-crystalline $Mg_3Al_2(SiO_4)_3$ pyrope with random orientation present similar pressure evolution of thermal conductivity; Λ is ~4.4 W $m^{-1} K^{-1}$ at ambient conditions and increases with pressure to Λ=9–10 W $m^{-1} K^{-1}$ at ~20 GPa. Since the difference in their thermal conductivity is smaller or comparable to the data uncertainty (~8–15%, see Methods), our measurements indicate that the presence of <700 wt. ppm water in pyrope does not influence the thermal conductivity, even at pressures as high as 20 GPa.

On the other hand, the Λ of single-crystalline $(Ca_{0.986}Fe_{0.014})_3Al_2(SiO_4)_3$ grossular with random orientation and ~5500 wt. ppm water (blue squares in Fig. 1(a)) is ~4.1 W $m^{-1} K^{-1}$at ambient conditions, ~40% smaller than the nominally dry $Ca_3Al_2(SiO_4)_3$ grossular (Slack and Oliver 1971), suggesting that the incorporation of ~5500 wt. ppm water acting as impurities in grossular could reduce its thermal conductivity. We note that the critical threshold for the amount of water that starts to decrease the thermal conductivity of a mineral remains poorly constrained, since it depends on a number of properties of the mineral. Nevertheless, our present results are consistent with previous studies (Chang et al. 2017; B. Zhang et al. 2019; Marzotto et al. 2020), which showed that when the water content is larger than approximately 1000–2000 wt. ppm, the thermal conductivity of a mineral could be significantly reduced. Compared to the pyrope data, the grossular is ~10–15% less thermally-conductive at ambient and low pressure regime, presumably due to the heavier cation of Ca and large amounts of water. After ~8 GPa, however, the Λ of grossular becomes essentially the same as the pyrope, suggesting that the application of pressure reduces the effects of end-member element and hydration on their thermal conductivity.

This is the peer-reviewed, final accepted version for American Mineralogist, published by the Mineralogical Society of America.
The published version is subject to change. Cite as Authors (Year) Title. American Mineralogist, in press.
DOI: https://doi.org/10.2138/am-2023-8953. http://www.minsocam.org/

Interestingly, a similar behavior is also observed in the Λ of randomly-oriented, single-crystalline $(Mg_{0.44}Fe_{0.45}Ca_{0.1}Mn_{0.01})_3Al_2(SiO_4)_3$ pyrope-almandine solid solution (green open triangles in Fig. 1(a)). With the large amounts of Fe cations that strongly scatter phonons for thermal energy transport, the Λ of pyrope-almandine solid solution at ambient conditions is decreased down to 3.4 W m^{-1} K^{-1}, in good agreement with that of the pyrope-almandine solid solution (Slack and Oliver 1971) with a chemical composition similar to our sample. With increasing pressure, its thermal conductivity difference from the pyrope and grossular is reduced; again, after ~8 GPa, all the three Al-garnets show nearly the same thermal conductivity. Note that (Marquardt et al. 2009) found that the thermal conductivity of garnet solid solutions exhibits lower values at intermedium compositions than the end member. Nevertheless, such effect is minimized with increasing temperature. Here our present data suggest that high pressure plays a similar role in reducing the thermal conductivity difference among the distinct chemical compositions. Moreover, since the thermal conductivity of a material can be estimated as $\Lambda=\Sigma_i(1/3)C_iV_i^2\tau_i$, where the C_i, V_i, and τ_i are the heat capacity, sound velocity, and relaxation time of the *i*-th phonon mode, respectively, the similar pressure evolution of thermal conductivity among the three Al-garnets can thus be primarily accounted for by their similar heat capacity and sound velocity at high pressures (Haselton and Newton 1980; Hofmeister and Chopelas 1991; Duan et al. 2019).

Figure 1(b) describes the temperature dependence of Λ of Al-garnets at a fixed pressure and 300–773 K. Though our measurement temperature was increased to only 773 K, clear and consistent dependences among these Al-garnets were observed. As expected, the Λ of all three Al-garnets decreases with temperature, a typical behavior of mantle silicate minerals (Xu et al. 2004; Hsieh et al. 2018, 2022b; Y. Zhang et al. 2019). To better quantify their temperature dependences,

This is the peer-reviewed, final accepted version for American Mineralogist, published by the Mineralogical Society of America.
The published version is subject to change. Cite as Authors (Year) Title. American Mineralogist, in press.
DOI: https://doi.org/10.2138/am-2023-8953. http://www.minsocam.org/

we assumed that their Λ can be phenomenologically modeled as $\Lambda(T)=\beta T^n$, where β is a normalization constant. The temperature exponent n is then determined by a linear regression slope in the $\ln\Lambda$–$\ln T$ plot. We found that for pyrope with ~700 wt. ppm water, n_{pyrope}= -0.49(±0.09) at 6 GPa and -0.47(±0.06) at 17 GPa. For grossular, $n_{\text{grossular}}$= -0.43(±0.05) at 3 GPa and -0.47(±0.05) at 17.6 GPa. The dependence of pyrope-almandine solid solution, $n_{\text{pyrope-almandine}}$, was fitted to be -0.48(±0.1) at 6.2 GPa. Though the measurement pressure and chemical composition are different, these n values are close to the theoretical value of -0.5 for an impurity-bearing dielectric material (Klemens 1960), and are in good agreement with those for Fe-bearing olivine determined by previous experiments (Xu et al. 2004; Y. Zhang et al. 2019).

The present experimental results advance our understanding of how the thermal conductivity of garnets influences the thermal structures of the pyrolitic mantle and subducting slabs. To this end, we first model the thermal conductivity of the three Al-garnets along a representative geotherm of the pyrolitic mantle and a subducting slab. The geotherm of the pyrolitic mantle was taken from (Katsura et al. 2010) and that of a subducting slab was assumed to be 800 K colder. Based on our data for the pressure and temperature dependences (Fig. 1(a) and (b), respectively), we plot the modelled thermal conductivity of Al-garnets as a function of depth in the pyrolitic mantle and a subducting slab, see Fig. 2(a) and (b), respectively. In the pyrolitic mantle, as expected, the thermal conductivities of the Al-garnets show similar profiles, increasing from ~2.2 W m^{-1} K^{-1} at 150 km depth to ~3.7 W m^{-1} K^{-1} at 660 km depth. Note that these profiles are smaller than that of dry olivine (Chang et al. 2017) and dry ringwoodite (Marzotto et al. 2020) (orange and navy dashed curves in Fig. 2(a), respectively). Since the presence of water reduces the thermal conductivity of ringwoodite (Marzotto et al. 2020), depending on the water content, the

profile of hydrous ringwoodite could be comparable or even smaller than the Al-garnets. For instance, the navy dotted curve in Fig. 2(a) is for ringwoodite incorporated with 1.73 wt% water.

On the other hand, previous modelling of a slab's thermal conductivity during subduction typically replaced the garnet by olivine due to the lack of garnet's thermal conductivity data, e.g., (Hsieh et al. 2022b, 2022a). Our present thermal conductivity profiles for the Al-garnets significantly advance the data modelling: here we assume the subducting lithosphere is made of 40 vol% of pyrope garnet and 60 vol% of olivine (or ringwoodite in the transition zone), and also assume the basaltic crust is made of 90 vol% of grossular garnet (Wood et al. 2013) and 10 vol% of stishovite. The profiles of the basaltic crust and lithosphere (red and orange-navy dashed curves, respectively, in Fig. 2(b)) are both smaller than previously modelled (Hsieh et al. 2022b, 2022a) by ~10–30%, depending on the depth and water content in ringwoodite. The less thermally conductive slab that we find here suppresses the heat transfer through the subducting slab. This would contribute to a colder temperature profile along with higher density and larger negative buoyancy than previously expected, stabilizing the slab minerals as well as influencing the local seismic features and subduction dynamics.

Implications

To summarize, we combined the TDTR and EHDAC to characterize the effects of pressure, temperature, and composition on the thermal conductivity of Al-garnets. Our new data modelling shows that throughout the depths of upper mantle and transition zone, the thermal conductivity profiles of the Al-garnets we studied here are nearly the same; their profiles, however, are smaller than the dry olivine and dry ringwoodite, yet larger than the hydrous ringwoodite containing 1.73 wt% water. The limited effects of end-member chemistry on the thermal conductivity of these Al-

garnets suggest that their profiles could reasonably represent the conductivity of the complex, variable garnet solid solutions in Earth's deep interior. These findings offer important mineral physics properties beneficial to the geodynamics simulations where the thermal conductivity of garnets were largely unknown (Hsieh et al. 2022a, 2022b). Combined with dynamics modelling, future experimental studies on the thermal conductivity of other mantle minerals, such as majorite, a variety of pyroxenes, and davemaoite, under relevant chemical composition and high *P-T* conditions will enable more comprehensive understanding of the complex thermochemical structure, seismic discontinuity, and evolution of the pyrolitic mantle and subducting slabs. Since a variety of synthetic nonsilicate garnets have been widely used in modern lasers and electronic devices, garnets' thermal conductivity plays a critical role in affecting the thermal management and long-term performance of these devices. Our results for the effects of composition and temperature on the thermal conductivity of natural garnets would therefore bring important benefits to future advanced design and fabrication of devices based on synthetic garnets for laboratory and industrial technology.

Data availability

Our data are stored in the Zenodo repository: https://zenodo.org/record/7306225#.Y2sOVnZBw2y

Acknowledgements

We thank Chih-Yu Liu, Shao-Yu Ho, Chao-Hsi Wang for their help at Academia Sinica in the early stage of the research. This work was supported by the Academia Sinica and the National Science and Technology Council (NSTC) of Taiwan, Republic of China, under Contract AS-IA-111-M02 and 110-2628-M-001-001-MY3.

Author Contributions

W.P.H. conceived and designed the project. Y.P.H., Y.C.T., C.H.L., and W.P.H. conducted experiments and analyzed data. Y.C.T., C.H.L., and W.P.H. wrote, reviewed, and commented on the manuscript.

Competing interests

The authors declare no competing interests.

References

Arimoto, T., Gréaux, S., Irifune, T., Zhou, C., and Higo, Y. (2015) Sound velocities of Fe3Al2Si3O12 almandine up to 19 GPa and 1700 K. Physics of the Earth and Planetary Interiors, 246, 1–8.

Babuška, V., Fiala, J., Kumazawa, M., Ohno, I., and Sumino, Y. (1978) Elastic properties of garnet solid-solution series. Physics of the Earth and Planetary Interiors, 16, 157–176.

Baima, J., Ferrabone, M., Orlando, R., Erba, A., and Dovesi, R. (2016) Thermodynamics and phonon dispersion of pyrope and grossular silicate garnets from ab initio simulations. Physics and Chemistry of Minerals, 43, 137–149.

Cahill, D.G. (2004) Analysis of heat flow in layered structures for time-domain thermoreflectance. Review of Scientific Instruments, 75, 5119–5122.

Cahill, D.G., Braun, P. V, Chen, G., Clarke, D.R., Fan, S., Goodson, K.E., Keblinski, P., King, W.P., Mahan, G.D., Majumdar, A., and others (2014) Nanoscale thermal transport. II. 2003–2012. Applied Physics Reviews, 1, 011305.

Chang, Y.-Y., Hsieh, W.-P., Tan, E., and Chen, J. (2017) Hydration-reduced lattice thermal conductivity of olivine in Earth's upper mantle. Proc. Natl. Acad. Sci. USA, 114, 4078.

Chen, B., Hsieh, W.-P., Cahill, D.G., Trinkle, D.R., and Li, J. (2011) Thermal conductivity of compressed H2O to 22 GPa: A test of the Leibfried-Schlömann equation. Physical Review B, 83, 132301.

Conrad, P.G., Zha, C.S., Mao, H.K., and Hemley, R.J. (1999) The high-pressure, single-crystal elasticity of pyrope, grossular, and andradite. American Mineralogist, 84, 374–383.

Dai, L., and Karato, S. ichiro (2009) Electrical conductivity of pyrope-rich garnet at high temperature and high pressure. Physics of the Earth and Planetary Interiors, 176, 83–88.

Davies, G.F. (1988) Ocean bathymetry and mantle convection 1. Large-scale flow and hotspots. Journal of Geophysical Research, 93, 10467.

Dewaele, A., Loubeyre, P., and Mezouar, M. (2004) Equations of state of six metals above 94 GPa. Physical Review B, 70, 094112.

Duan, L., Wang, W., Wu, Z., and Qian, W. (2019) Thermodynamic and Elastic Properties of Grossular at High Pressures and High Temperatures: A First-Principles Study. Journal of Geophysical Research: Solid Earth, 124, 7792–7805.

Eberle, M.A., Grasset, O., and Sotin, C. (2002) A numerical study of the interaction between the mantle wedge, subducting slab, and overriding plate. Physics of the Earth and Planetary Interiors, 134, 191–202.

Erba, A., Mahmoud, A., Belmonte, D., and Dovesi, R. (2014) High pressure elastic properties of minerals from ab initio simulations: The case of pyrope, grossular and andradite silicate garnets. Journal of Chemical Physics, 140, 124703.

Fan, D., Lu, C., Xu, J., Yan, B., Yang, B., and Chen, J. (2017) Effects of water on P-V-T equation of state of pyrope. Physics of the Earth and Planetary Interiors, 267, 9–18.

Galkin, V., and Gartvich, Y. (2015) Thermal expansion and evaluation of almandine heat capacity. Journal of Thermal Analysis and Calorimetry, 122, 1239–1244.

Giesting, P.A., Hofmeister, A.M., Wopenka, B., Gwanmesia, G.D., and Jolliff, B.L. (2004) Thermal conductivity and thermodynamics of majoritic garnets: Implications for the transition zone. Earth and Planetary Science Letters, 218, 45–56.

Gillet, P., Fiquetw, G., Malézieux, J.M., and Geiger, C.A. (1992) High-pressure and high-temperature Raman spectroscopy of end-member garnets: pyrope, grossular and andradite. European Journal of Mineralogy, 4, 651–664.

Gréaux, S., Kono, Y., Nishiyama, N., Kunimoto, T., Wada, K., and Irifune, T. (2011a) P-V-T equation of state of Ca3Al2Si3O12 grossular garnet. Physics and Chemistry of Minerals, 38, 85–94.

Gréaux, S., Nishiyama, N., Kono, Y., Gautron, L., Ohfuji, H., Kunimoto, T., Menguy, N., and Irifune, T. (2011b) Phase transformations of Ca3Al2Si3O12 grossular garnet to the depths of the Earth's mantle transition zone. Physics of the Earth and Planetary Interiors, 185, 89–99.

Guo, J., Zhang, Ruixin, Wang, D., and Zhang, Rui (2022) Thermal Conductivity and Thermal Diffusivity of Talc at High Temperature and Pressure With Implications for the Thermal Structure of Subduction Zones. Journal of Geophysical Research: Solid Earth, 127, e2021JB023425.

Haselton, H.T., and Newton, R.C. (1980) Garnets and Their Stabilities at High Temperatures and High Pressures. J . Geophys. Res., 85, 6973–6982.

Hofmeister, A.M. (2006) Thermal diffusivity of garnets at high temperature. Physics and Chemistry of Minerals, 33, 45–62.

Hofmeister, A.M., and Branlund, J.M. (2015) Thermal Conductivity of the Earth, 583–608 p. Treatise on Geophysics: Second Edition Vol. 2. Elsevier B.V.

Hofmeister, A.M., and Chopelas, A. (1991) Thermodynamic properties of pyrope and grossular from vibrational spectroscopy. American Mineralogist, 76, 880–891.

Horai, K. (1971) Thermal Conductivity of Rock-Forming Minerals. J . Geophys. Res., 76, 1278.

Hsieh, W.-P. (2021) High-pressure thermal conductivity and compressional velocity of NaCl in B1 and B2 phase. Scientific Reports, 11, 21321.

Hsieh, W.-P., Chen, B., Li, J., Keblinski, P., and Cahill, D.G. (2009) Pressure tuning of the thermal conductivity of the layered muscovite crystal. Physical Review B, 80, 180302.

Hsieh, W.-P., Deschamps, F., Okuchi, T., and Lin, J.-F. (2017) Reduced lattice thermal conductivity of Fe-bearing bridgmanite in Earth's deep mantle. J . Geophys. Res. Solid Earth, 122, 4900.

——— (2018) Effects of iron on the lattice thermal conductivity of Earth's deep mantle and implications for mantle dynamics. Proceedings of the National Academy of Sciences of the United States of America, 115, 4099.

Hsieh, W.-P., Goncharov, A.F., Labrosse, S., Holtgrewe, N., Lobanov, S.S., Chuvashova, I., Deschamps, F., and Lin, J. (2020) Low thermal conductivity of iron-silicon alloys at Earth's core conditions with implications for the geodynamo. Nature Communications, 11, 3332.

Hsieh, W.-P., Marzotto, E., Tsao, Y.C., Okuchi, T., and Lin, J.-F. (2022a) High thermal conductivity of stishovite promotes rapid warming of a sinking slab in Earth's mantle. Earth and Planet. Sci. Lett., 584, 117477.

Hsieh, W.-P., Marzotto, E., Ishii, T., Dubrovinsky, L., Aslandukova, A.A., Criniti, G., Tsao, Y., Lin, C., Tsuchiya, J., and Ohtani, E. (2022b) Low Thermal Conductivity of Hydrous Phase D Leads to a Self-Preservation Effect Within a Subducting Slab. Journal of Geophysical Research: Solid Earth, 127, e2022JB024556.

Hsieh, W.-P., Tsao, Y., and Lin, C. (2022c) Thermal Conductivity of Helium and Argon at High Pressure and High Temperature. Materials, 15, 6681.

Hu, Y., Wu, Z., Dera, P., and Bina, C. (2016) Thermodynamic and elastic properties of pyrope at high pressure and high temperature by first-principles calculations. Journal of Geophysical Research, 121, 6462.

Jacobsen, S.D. (2006) Effect of Water on the Equation of State of Nominally Anhydrous Minerals. Reviews in Mineralogy and Geochemistry, 62, 321–342.

Jiang, F., Speziale, S., and Duffy, T.S. (2004) Single-crystal elasticity of grossular- and almandine-rich garnets to 11 GPa by Brillouin scattering. Journal of Geophysical Research: Solid Earth, 109, B10210.

Kang, K., Koh, Y.K., Chiritescu, C., Zheng, X., and Cahill, D.G. (2008) Two-tint pump-probe measurements using a femtosecond laser oscillator and sharp-edged optical filters. The Review of scientific instruments, 79, 114901.

Katsura, T., Yoneda, A., Yamazaki, D., Yoshino, T., Ito, E., Suetsugu, D., Bina, C., Inoue, T., Wiens, D., and Jellinek, M. (2010) Adiabatic temperature profile in the mantle. Physics of the Earth and Planetary Interiors, 183, 212–218.

Kawai, K., and Tsuchiya, T. (2012) First principles investigations on the elasticity and phase stability of grossular garnet. Journal of Geophysical Research: Solid Earth, 117, B02202.

——— (2015) Elasticity and phase stability of pyrope garnet from ab initio computation. Physics of the Earth and Planetary Interiors, 240, 125–131.

Klemens, P. (1960) Thermal Resistance due to Point Defects at High Temperatures. Physical Review, 119, 507–509.

Kolesov, B.A., and Geiger, C.A. (1998) Raman spectra of silicate garnets. Physics and Chemistry of Minerals, 25, 142–151.

Kono, Y., Gréaux, S., Higo, Y., Ohfuji, H., and Irifune, T. (2010) Pressure and temperature dependences of elastic properties of grossular garnet up to 17 GPa and 1 650 K. Journal of Earth Science, 21, 782–791.

Marquardt, H., Ganschow, S., and Schilling, F.R. (2009) Thermal diffusivity of natural and synthetic garnet solid solution series. Physics and Chemistry of Minerals, 36, 107–118.

Marzotto, E., Hsieh, W.P., Ishii, T., Chao, K.H., Golabek, G., Thielmann, M., and Ohtani, E. (2020) Effect of Water on Lattice Thermal Conductivity of Ringwoodite and Its Implications for the Thermal Evolution of Descending Slabs. Geophys. Res. Lett., 47, e2020GL087607.

Ohta, K., Yagi, T., Taketoshi, N., Hirose, K., Komabayashi, T., Baba, T., Ohishi, Y., and Hernlund, J. (2012) Lattice thermal conductivity of MgSiO3 perovskite and post-perovskite at the core–mantle boundary. Earth and Planetary Science Letters, 349–350, 109–115.

Ohta, K., Yagi, T., Hirose, K., and Ohishi, Y. (2017) Thermal conductivity of ferropericlase in the Earth's lower mantle. Earth and Planetary Science Letters, 465, 29–37.

Ono, S., Ito, E., and Katsura, T. (2001) Mineralogy of subducted basaltic crust (MORB) from 25 to 37 GPa, and chemical heterogeneity of the lower mantle. Earth and Planetary Science Letters, 190, 57–63.

Osako, M., Ito, E., and Yoneda, A. (2004) Simultaneous measurements of thermal conductivity and thermal diffusivity for garnet and olivine under high pressure. Physics of the Earth and Planetary Interiors, 143, 311–320.

Ringwood, A.E. (1991) Phase transformations and their bearing on the constitution and dynamics of the mantle. Geochimica et Cosmochimica Acta, 55, 2083–2110.

Schmidt, A., Chiesa, M., Chen, X., and Chen, G. (2008) An optical pump-probe technique for measuring the thermal conductivity of liquids. Review of Scientific Instruments, 79, 064902.

Slack, G.A., and Oliver, D.W. (1971) Thermal conductivity of garnets and phonon scattering by rare-earth ions. Physical Review B, 4, 592–609.

Wood, B.J., Kiseeva, E.S., and Matzen, A.K. (2013) Garnet in the earth's mantle. Elements, 9, 421–426.

Xu, Y., Shankland, T.J., Linhardt, S., Rubie, D.C., Langenhorst, F., and Klasinski, K. (2004) Thermal diffusivity and conductivity of olivine, wadsleyite and ringwoodite to 20 GPa and 1373 K. Physics of the Earth and Planetary Interiors, 143, 321–336.

Zhang, B., Ge, J., Xiong, Z., and Zhai, S. (2019) Effect of Water on the Thermal Properties of Olivine With Implications for Lunar Internal Temperature. Journal of Geophysical Research: Planets, 124, 3469–3481.

Zhang, B., Fei, H., Ge, J., Zeng, L., and Xia, Q. (2022) Crustal melting in orogenic belts revealed by eclogite thermal properties. Nature Communications, 13, 4673.

Zhang, Y., Yoshino, T., Yoneda, A., and Osako, M. (2019) Effect of iron content on thermal conductivity of olivine with implications for cooling history of rocky planets. Earth and

Planetary Science Letters, 519, 109–119.

This is the peer-reviewed, final accepted version for American Mineralogist, published by the Mineralogical Society of America.
The published version is subject to change. Cite as Authors (Year) Title. American Mineralogist, in press.
DOI: https://doi.org/10.2138/am-2023-8953. http://www.minsocam.org/

Figure captions

Fig. 1. (a) Thermal conductivity of pyrope, grossular, and pyrope-almandine solid solution at high pressure and room temperature. For each single-crystalline mineral with random orientation, we performed multiple runs of measurements that show consistent results, suggesting that their thermal conductivity is insensitive to the crystal orientation. Overall the three Al-garnets exhibit similar thermal conductivity over the pressure range we studied. The data uncertainty is ~8% before 10 GPa and ~15% at 10–25 GPa. Literature results for pyrope (Marquardt et al. 2009) and hydrous grossular (Hofmeister and Branlund 2015) (each contains a small amounts of other garnets) at ambient pressure are plotted as open black circle and open blue square, respectively, for comparison. (b) Temperature dependence of the thermal conductivity of Al-garnets at a given pressure. Assuming the thermal conductivity (with an analysis uncertainty of ~15%) scales with T^n, the exponent value for each case is determined as n_{pyrope}= -0.49(±0.09) at 6 GPa (red squares, Py-6 GPa) and n_{pyrope}=-0.47(±0.06) at 17 GPa (red circles, Py-17 GPa), $n_{\text{grossular}}$= -0.43(±0.05) at 3 GPa (blue triangles, Gr-3 GPa) and $n_{\text{grossular}}$= -0.47(±0.05) at 17.6 GPa (blue circles, Gr-17.6 GPa), and $n_{\text{pyrope-almandine}}$= -0.48(±0.1) at 6.2 GPa (green squares, PyAl-6.2 GPa).

Fig. 2. Thermal conductivity profiles of Al-garnets along (a) mangle geotherm and (b) slab geotherm. (a) In the pyrolitic mantle, the thermal conductivity of all Al-garnets (each has the same color as in Fig. 1(a)) is smaller than the dry olivine (orange dashed curve)(Chang et al. 2017) and dry ringwoodite (dry Rw, navy dashed curve)(Marzotto et al. 2020), but larger than the hydrous Rw containing 1.73 wt% water (hy Rw, navy dotted curve)(Marzotto et al. 2020). (b) Within a subducting slab, the basaltic crust (red dashed curve) is relatively thermally-conductive, since it is assumed to contain 10 vol% stishovite with an exceptionally high thermal conductivity(Hsieh et al. 2022a), along with 90 vol% grossular garnet. The orange dashed curve is the thermal conductivity of a subducting lithosphere composed of pyrope with dry olivine, while the navy dashed and navy dotted curves are for a subducting lithosphere made of pyrope with dry Rw and pyrope with hydrous Rw, respectively. The profile for grossular garnet (blue curve) is plotted for comparison.

This is the peer-reviewed, final accepted version for American Mineralogist, published by the Mineralogical Society of America.
The published version is subject to change. Cite as Authors (Year) Title. American Mineralogist, in press.
DOI: https://doi.org/10.2138/am-2023-8953. http://www.minsocam.org/

462

463 Figure 1

464

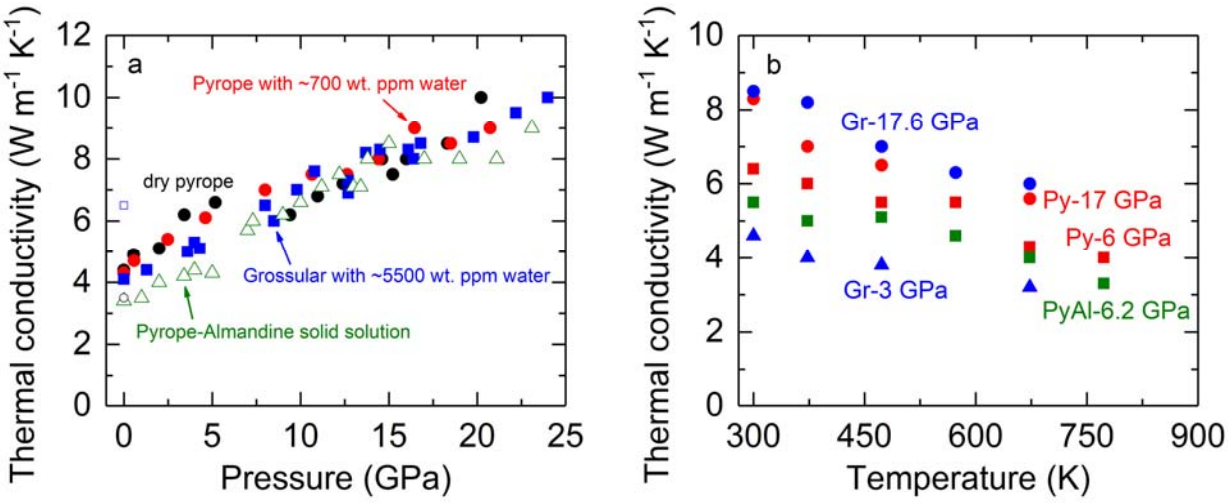

465

466

467

468

469 Figure 2

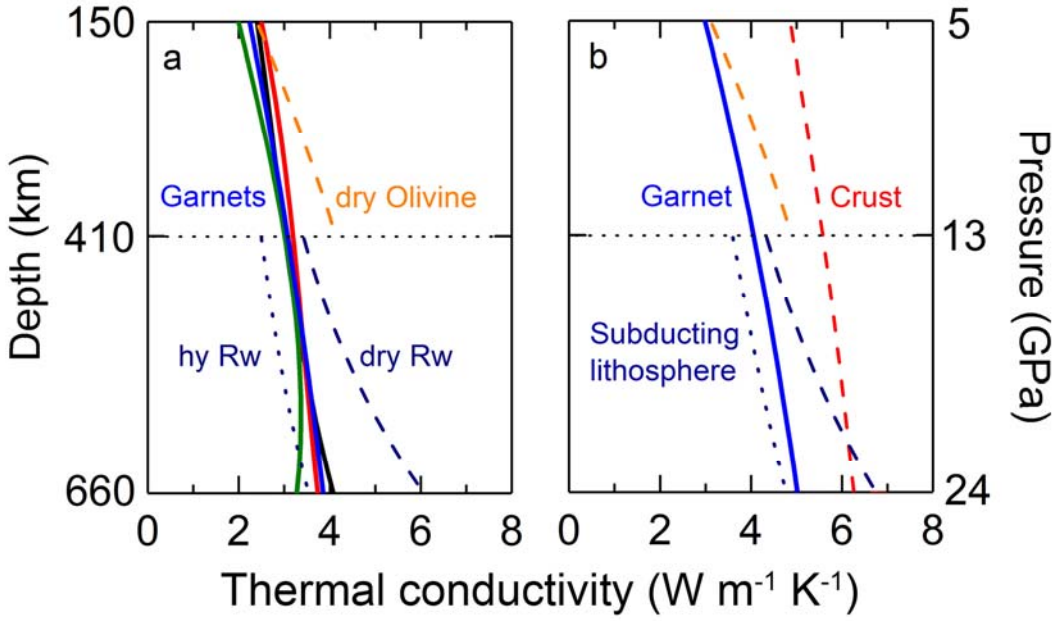

470